Mixed-Domain Simulation of Step-Functional Voltammetry with an Insoluble Species for Optimization of Chemical Microsystems

Steven M. Martin, Timothy D. Strong, Fadi H. Gebara, Richard B. Brown

Department of Electrical Engineering and Computer Science
University of Michigan, Ann Arbor, MI 48109
{stevenmm, strongtd, fadi, brown}@umich.edu

ABSTRACT

Microinstruments with integrated sensors and electronics are well adapted for remote environmental monitoring applications. Optimization of these microinstruments, however, has been difficult due to a previous lack of mixed-domain simulation environments. This work presents a complete electrode model for step-functional voltammetry with an insoluble species. The model includes the electrochemical response, sensor parasitics, sensor noise, and electrical instrumentation, and can be simulated in a standard electronic CAD environment. The simulation results are verified against experimental data taken using microfabricated sensors. Finally, the design environment is used to analyze system-wide design trade-offs.

Keywords: mixed-domain simulation, voltammetry, microsystem design, toxic metals

1 INTRODUCTION

An important application of electrochemical microsensors is the analysis of trace levels of toxic metals [1]. Electrochemical analyses using anodic stripping voltammetry (ASV) can provide detection limits down to 10 picomolar for some heavy metals [2]. For remote monitoring applications, it may be necessary to miniaturize or even integrate the electronic instrumentation for ASV directly with the sensors [1]. Furthermore, the long-term deployment of these microinstruments requires that both sensor and electronics be optimized to operate on small power budgets, occupy little area, and provide adequate detection limits. Unfortunately, the trade-offs among these goals are not always obvious and simulation tools for system optimization have not existed, making chemical microinstrument optimization, or even designing to specification, a difficult task at best.

While physics-based models for sensor parasitics [3], sensor noise sources [4,5], and electrochemical faradaic currents [6] have previously been developed, there has been limited work in combining the components into a cohesive model and analyzing the trade-offs for detecting heavy metals on bare electrodes. Morgan [4] performed analyses for voltammetric sensors and their instrumentation when used to detect analytes with soluble products–a problem which has a closed-form solution. Electrochemical detection of heavy metals, however, involves voltammetry with a species that has an insoluble product. Voltammetry at bare electrodes with an insoluble species has no closed-form solution and requires numerical methods to solve.

This work presents a complete model and method for the system-level simulation of a mixed-domain, bare-electrode, heavy-metal microdetector. First, a sensor model is presented which combines linear electrical components and Verilog-AMS code to model the electrode process, parasitics, and noise. The model is then combined with schematics of the instrumentation and simulated using the circuit simulator, *Spectre*®. The model is verified against experimental results, and design optimization analyses employing the simulation environment are discussed.

2 SENSOR FUNDAMENTALS

2.1 Electrode Processes with Insoluble Species

Voltammetry is an electrochemical technique in which a series of potentials, E, are applied between an electrode and solution, and the resulting faradaic current, I_f, is measured [2]. This electrode is called the working electrode (WE), and the faradaic current is given by

$$I_f(t) = nFAD_o \left.\frac{\partial C_o(x,t)}{\partial x}\right|_{x=0} \tag{1}$$

where x is the distance away from the electrode surface, n is the number of electrons transferred in the redox reaction, F is Faraday's constant, A is the area of the electrode, and D_o and C_o are the diffusion coefficient and concentration of the oxidized form of the analyte, respectively. The concentration change is defined by Fick's 2nd Law of Diffusion which is the partial differential equation,

$$\frac{\partial C_o(x,t)}{\partial t} = D_o\left(\frac{\partial^2 C_o(x,t)}{\partial x^2}\right). \tag{2}$$

The boundary conditions for voltammetry with an insoluble species on a bare electrode were first reported in [6] for a cyclic voltammetry experiment. Altering the boundary conditions of [6] to apply to any arbitrary step-functional voltammetry yields the three boundary conditions:

$$\left.C_o(x,t)\right|_{\substack{t=0\\x\geq 0}} = C_o^* \tag{3}$$

$$\lim_{x\to\infty} C_o(x,t) = C_o^* \qquad \text{for } t \geq 0 \tag{4}$$

$$\left.\frac{-D}{K_s}\frac{\partial C_o}{\partial x}\right|_{x=0} = a\exp\left[\frac{\beta nF}{RT}(E-E^0)\right] - C_o(0,t)\exp\left[\frac{-\alpha nF}{RT}(E-E^0)\right] \quad (5)$$

where $a = a_\infty\left\{1-\exp\left[-\gamma\left(Q-\int_0^t i\,dt\right)\right]\right\}$. (6)

C_o^* is the initial concentration, K_s is the heterogeneous rate constant for the redox reaction, a is the activity of the insoluble species on the electrode, α and β are transfer coefficients, E^0 is the reduction potential of the analyte, Q is the total charge of the moles plated onto the electrode, R is the gas constant, γ is the activity coefficient, and T is temperature. This partial differential equation has no closed-form solution but can be solved numerically using a difference equation technique. The solution method used here follows the derivation presented in [6] except that a step-functional input waveform is assumed instead of a cyclic waveform. This slightly alters the change of variables in the derivation.

2.2 Parasitics

Application of the desired potential to the test solution requires the use of additional electrodes. Typical microamperometric sensors consist of three electrodes—the auxiliary (AE), reference (RE), and working electrodes (WE) [3]. Unfortunately, each of these electrodes introduces parasitics into the electrochemical cell. These parasitics can be adequately modeled using linear electrical components as shown in Figure 1 [3]. C_a and C_w represent the double-layer capacitances of both the AE and WE respectively, and are given by [7]

$$C_j \approx 20\left(\frac{\mu F}{cm^2}\right)\cdot A_j \quad (7)$$

for each electrode j. R_s and R_t represent the solution resistance between the various electrodes and are given by [3]

$$R_j = \frac{d_j}{\kappa A_j} \quad (8)$$

where d_j is the distance between the two electrodes and κ is the solution conductivity. The charge transfer impedances at the AE and WE, R_a and R_w, are given by [2]

$$R_j = \frac{1}{i_{o_j} nF A_j} \quad (9)$$

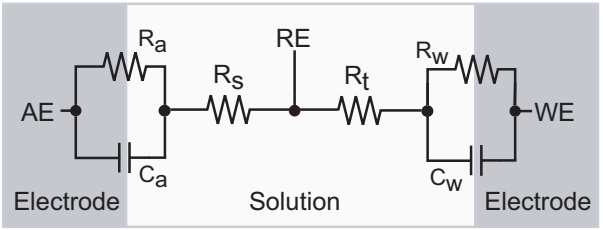

Figure 1: Parasitics and noise model of a three-electrode voltammetric sensor.

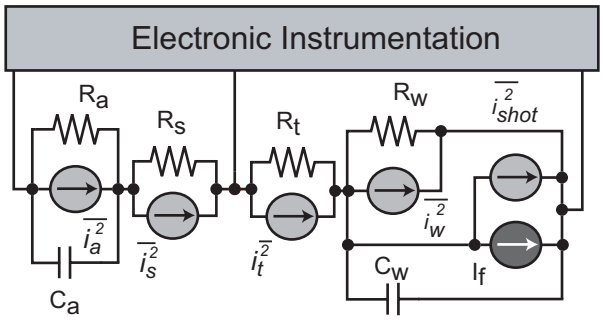

Figure 2: Microsystem model including faradaic current source, sensor parasitics, noise sources, and electronic instrumentation.

where i_o is the equilibrium current density. Of the parasitics, C_w is of utmost concern since any current needed to charge/discharge the double-layer capacitance is summed with the concentration dependent faradaic current. Large charging currents mask the desired redox current and lead to poor detection limits. Equations (7)-(9) demonstrate that the parasitics have dependencies on the areas of the electrodes and their separations. Furthermore, the relationships between the various parasitics and their areas create trade-offs in electrode sizing.

2.3 Noise

Noise in the electrochemical cell is generated from both the faradaic current and from the parasitics. Similar to any resistor, the solution impedances and charge transfer resistances produce a thermal current noise given by

$$\overline{i^2_{thermal}} = \frac{4kTB}{R} \quad (10)$$

where k is the Boltzmann constant, T is temperature, B is the bandwidth, and R is the impedance [4]. Additional noise in the form of shot noise arises from the discrete electron transfer from ion in solution to electrode and is given by

$$\overline{i^2_{shot}} = 2qB(I_f + I_c) \quad (11)$$

where q is the charge of an electron and I_c is the charging current [4]. In the electrical model, these noise sources can be added in parallel with their respective sources. Since the magnitudes of R, I_f, and I_c are dependent on area, electrode dimensions directly affect the total noise generated in the system.

3 SYSTEM SIMULATION

3.1 System Model

With the various components of the sensor defined, the modeling and simulation of the entire chemical microsystem can be achieved. Combining the faradaic current, parasitics, noise sources, and necessary electronics yields the electrically equivalent model shown in Figure 2. The electrical simulator *Spectre*® was chosen as the simulation environment since it can operate on both electrical netlists and Verilog-AMS code. The electrical parts of the system model

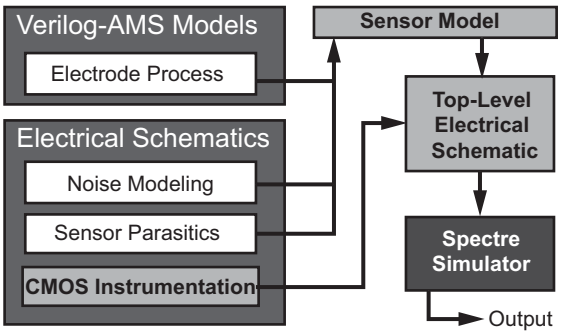

Figure 3: Design environment for the simulation of the heavy-metal microdetector.

were implemented in schematic form with variables representing key design parameters like electrode areas and separation. Verilog-AMS was used to find the numerical solution to step-functional voltammetry with insoluble species present. Noise analysis was accomplished using the standard *Spectre*® noise solver with inputs derived from the transient simulations of sensor currents. Figure 3 details the implementation of the system model for mixed-domain simulation.

3.2 Simulation Time

Since the solution of the partial differential equation defining the faradaic current involves solving a difference equation in two variables (x and t), the simulation time is on the order of N^2 as shown in Figure 4. To speed the simulation, Δx and Δt can be scaled, but scaling these values ultimately degrades the accuracy of the solution. Figure 4 shows the percent error incurred by scaling Δx and Δt.

4 VERIFICATION

To verify the accuracy of the simulation environment, results from the simulations were compared with experimental results. The experimental setup consisted of a microfabricated, 0.375mm^2 Pt working electrode [8], a saturated calomel reference electrode, and a Pt wire auxiliary electrode submerged in a solution of 10mM HNO_3, 10mM NaCl with various concentrations of Pb^{2+}. A commercial potentiostat (FAS2™ Femtostat, *Gamry Instruments*) was used to generate and record the voltammetric sweeps. The experiments were run in a faraday cage to limit the effects of noise on the system. Table 1 lists the simulator's input parameters.

Variable	Value	Description
A_w	0.00375	Area of working electrode (cm^2)
A_a	1	Area of auxiliary electrode (cm^2)
κ	0.01	Conductivity of solution (S/cm)
d_w	1	Distance between RE and WE (cm)
d_a	2	Distance between RE and AE (cm)
B	100	Circuit bandwidth (kHz)
Q	0	Initial charge deposited (C)
D_o	9.9e-6	Pb^{2+} diffusion coefficient (cm2/s)
n	2	Electrons transferred
K_s	5e-3	Rate constant (cm/s)
E^0	-0.5	Standard potential (V)
α, β	0.5	Transfer coefficients
γ	0.5	Activity coefficient
l	4000	Max diffusion distance (unitless)
N_x	1000	Number of Δx bins
$Max_{\Delta t}$	15	Maximum timestep (ms)

Table 1: Simulation parameters used.

Figure 5 shows the results of total electrolyzed charge versus initial concentration of Pb^{2+} during a cyclic voltammogram. Both the experimental and simulated data show a linear trend versus concentration and compare reasonably well. Figure 5 also shows the dynamic response of the system during a cyclic voltammetric sweep. The simulated and experimental waveforms have similar shapes, but the experimental peak current is larger than the simulation predicts. A simple fitting parameter will be added to the simulation in future experiments to correct this inaccuracy.

Figure 6 compares the individually normalized peak currents versus voltammetric scan rate during a linear sweep voltammogram. These curves were generated in 1mM Pb^{2+}.

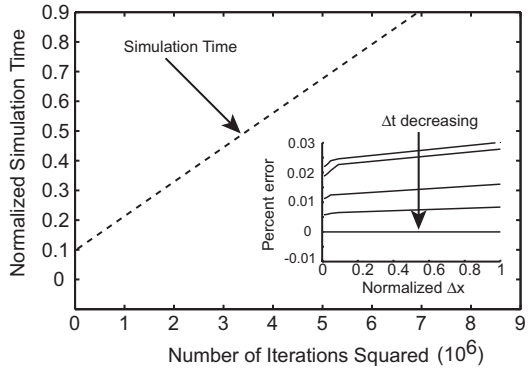

Figure 4: Normalized simulation time vs. the square of the number of discrete Δx and Δt bins chosen for solving the differential equation. (Inset) Percent error in the voltammetric peak current for various values of Δx and Δt.

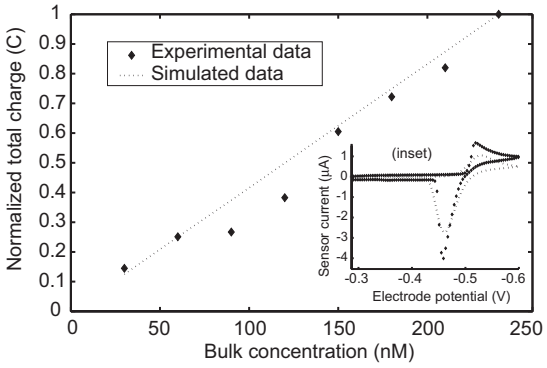

Figure 5: Comparison of simulated and experimental total electrolyzed charge during a cyclic voltammogram. (Inset) Dynamic response of simulation and experiment during a cyclic voltammogram.

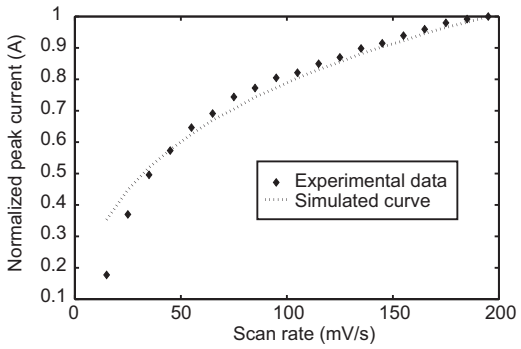

Figure 6: Comparison of simulated and experimental voltammetric peak current versus scan rate of the applied potential.

Again, the simulated and experimental results agree favorably. Finally, Figure 7 compares the individually normalized peak current versus deposition time [2] during ASV with linear scan stripping. The simulated curve has a natural logarithm shape due to the anticipated absence of stirring during deposition, while the experimental results show a more linear tendency. This discrepancy can be attributed to unwanted convection in the experimental setup during deposition.

5 MICROSYSTEM ANALYSIS

The design environment detailed here can be used to alter various system parameters and analyze their effects on overall system performance. One such analysis is the effect of the applied potential's scan rate on the signal-to-noise ratio of the system. The results of this analysis are given in Figure 8. The results show an increase in the total noise current as scan rate increases. This is due to the increasing charging currents required to charge/discharge the working electrode's double-layer capacitance. As verified in section 4, the faradaic current also increases with scan rate. The faradaic current, however, increases at a much slower rate than the total noise creating the signal-to-noise ratio curve shown. For the optimization of SNR, the simulations show that slow scan rates are better. The design environment presented is useful for all types of chemical microsystem optimization including power, area, bandwidth, and detection limit.

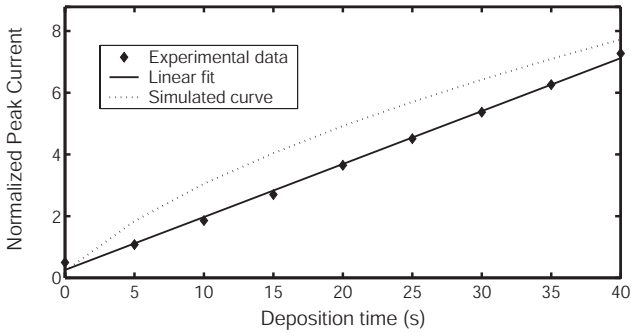

Figure 7: Comparison of simulated and experimental normalized peak current versus deposition time.

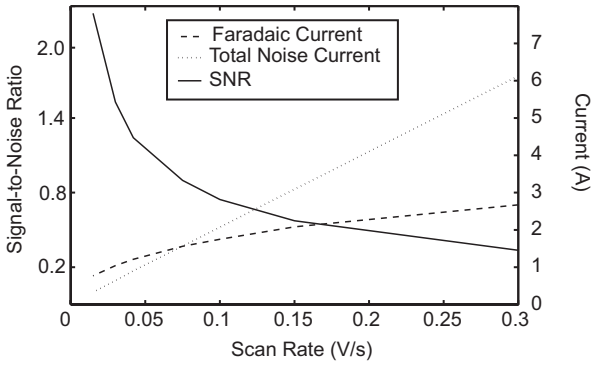

Figure 8: Simulation results for the analysis of signal-to-noise ratio versus scan rate for a heavy-metal microdetector.

6 CONCLUSION

A complete model for electron transfer between electrodes and analytes with insoluble products has been developed through the synthesis of several existing models. The model was implemented in Verilog-AMS and was simulated within the framework of a standard CAD tool allowing for complete mixed-domain simulation. Results were experimentally verified by analyzing Pb^{2+} on microfabricated Pt electrodes. The simulation environment was then used to investigate system-wide trade-offs. This work aids in the development of near optimal chemical microsystems. This optimization is required if microsystem technology is to become a cost-effective, environmental monitoring alternative.

ACKNOWLEDGEMENTS

This work was supported in part by the Engineering Research Centers Program of the US National Science Foundation under Award Number EEC-9986866 and under a National Science Foundation Graduate Research Fellowship.

REFERENCES

[1] S. Martin, T. Strong, F. Gebara, et. al., "Integrated Microtransducers and Microelectronics for Environmental Monitoring," *Proceedings of the 15th Biennial University/Government/Industry Microelectronics Symposium (UGIM 2003)*, Boise, ID, pp. 300-303, June 2003.

[2] P. Kissinger, and W. Heineman Eds. *Laboratory Techniques in Electroanalytical Chemistry Second Edition, Revised and Expanded*, Marcel Dekker, Inc., New York, 1996.

[3] A. Bard, and L. Faulkner, *Electrochemical Methods*, New York: John Wiley & Sons, 1980.

[4] D. Morgan, and S. Weber, "Noise and Signal-to-Noise Ratio in Electrochemical Detectors," *Analytical Chemistry*, vol. 56, pp. 2560-2567, 1984.

[5] R. VandenBerg, A. DeVos, and J. DeGoede, "Resistivity fluctuations in ionic solutions," in *8th Intl. Conf. on Noise in Physical Systems*, A. D'Amico, and P. Mazzetti, Eds., North Holland, New York, 1985.

[6] K. Brainina, *Stripping Voltammetry in Chemical Analysis*, John Wiley & Sons, New York, NY, 1974.

[7] M. Madou, and S. Morrison, *Chemical Sensing with Solid State Devices*, Academic Press, Inc., New York, 1989.

[8] M. Poplawski, H. Cantor, et.al., "Microfabricated amperometric biosensors," *Intl. Conf. on Solid-State Sensors and Actuators (Transducers '91)*, San Francisco, Ca, June24-28, 1991, pp. 51-53.